Carbon 121 (2017) 1–9

Contents lists available at ScienceDirect

Carbon

journal homepage: www.elsevier.com/locate/carbon

Facile growth of vertically-aligned graphene nanosheets via thermal CVD: The experimental and theoretical investigations

Huaping Wang [a, b], Enlai Gao [c], Peng Liu [d], Duanliang Zhou [d], Dechao Geng [a, b], Xudong Xue [a, e], Liping Wang [e], Kaili Jiang [d, **], Zhiping Xu [c, ***], Gui Yu [a, b, *]

[a] Beijing National Laboratory for Molecular Sciences, Institute of Chemistry, Chinese Academy of Sciences, Beijing 100190, PR China
[b] University of Chinese Academy of Sciences, Beijing 100049, PR China
[c] Applied Mechanics Laboratory, Department of Engineering Mechanics and Center for Nano and Micro Mechanics, Tsinghua University, Beijing 100084, PR China
[d] Department of Physics & Tsinghua-Foxconn Nanotechnology Research Center, Tsinghua University, Beijing 100084, PR China
[e] School of Materials Science and Engineering, University of Science and Technology Beijing, Beijing 100083, PR China

ARTICLE INFO

Article history:
Received 22 December 2016
Received in revised form
4 May 2017
Accepted 21 May 2017
Available online 22 May 2017

ABSTRACT

Owing to the distinctively morphological and structural features, vertically-aligned graphene nanosheets (VGs) possess many unique properties and hold great promise for applications in various fields. For controllable preparation and wide application of VGs, the establishing reliable growth method and profound understanding of the growth mechanism are of vital significance. Up to date, VGs are normally produced by plasma-enhanced chemical vapor deposition (PECVD) and it's considered that plasma is an indispensible factor for the vertical alignment of graphene sheets. Herein, for the first time, we report the facile and controllable VGs growth via a thermal CVD by precisely tuning growth parameters. Experimental observations in combination with detailed energy calculations reveal that the flow rate of carbon precursor determines the growth dynamics of graphene in CVD. This work offers a novel and reliable technique for VGs preparation and provides new insights into the intrinsic mechanism of vertical graphene growth. Furthermore, benefiting from the ultra-high density of edge sites, thin thickness, and outstanding electrical conductivity of VGs, the as-prepared VGs exhibit excellent field-emission performance such as ultra-low turn-on electric field and threshold field down to 1.07 and 1.65 V μm^{-1}, respectively.

1. Introduction

Vertically-aligned graphene nanosheets (VGs), or known as carbon nanowalls (CNWs), a type of three-dimensional (3D) graphene architecture which is formed by two-dimensional (2D) graphene nanosheets arranged perpendicularly to substrates, have attracted growing attentions in recent years [1–3]. Owing to the distinctively morphological and structural features, it possesses many unique electrical, chemical, and mechanical properties compared with its horizontal counterpart [4,5]. Based on those advanced functional properties, VGs hold great promise for a wide range of applications and remarkably expand the scope of 2D pristine graphene. For instance, attributed to the increased surface-to-volume ratio and high density of reactive surface sites, 3D vertical graphene sheets have been extensively studied for biological and chemical sensors [6–8]. The superior electrical conductivity and high specific surface area also make VGs an ideal candidate to fabricate high-performance supercapacitors [9–16]. Furthermore, the vertical orientation, sharp exposed edges and outstanding charge-transport properties endow VGs with exceptional electron field emission performance [17–23]. Besides, with the adjustable electrical conductivity, high surface area and fast electron transport channel, vertically-oriented graphene sheets can be exploited as excellent catalyst support for highly-efficient electrocatalysis [24,25]. Therefore, for the efficient use of such promising material, achieving a controllable preparation of VGs and gaining an in-depth understanding about formation mechanism play vital significance in both scientific and industrial aspects.

* Corresponding author.
** Corresponding author.
*** Corresponding author.
E-mail addresses: jiangkl@tsinghua.edu.cn (K. Jiang), xuzp@tsinghua.edu.cn (Z. Xu), yugui@iccas.ac.cn (G. Yu).

http://dx.doi.org/10.1016/j.carbon.2017.05.074
0008-6223/

Since from the first report of CNWs in 2002 during a carbon nanotubes growth process via microwave plasma-enhanced chemical vapor deposition (MPECVD) [2], VGs or CNWs are normally produced by plasma-based approaches [8,10,13,26–28]. Benefiting from its low-temperature and catalyst-free features, plasma-enhanced CVD (PECVD) has been proved to be a highly-efficient method for controllable VGs fabrication with various structures and diverse properties [1,6,9,15,29,30]. Although this method has been extensively applied to VGs research and several theoretical studies have been performed, the detailed growth mechanism of VGs involved in PECVD still remains elusive [27,31–33]. However, the precursor dissociation induced by the plasma is commonly considered to play a crucial role for the growth and alignment of VGs as the fact that VGs generally cannot produce in a thermal CVD [2]. In the PECVD system, it seems like that the fractional carbon-containing species and radicals generated in hydrocarbon plasma act as the building units for the VGs growth, but the actual mechanism and how plasma affects the vertical alignment of graphene are still unknown so far. For controllable preparation and wide application of VGs, the in-depth understanding of growth mechanism and more reliable growth method should be provided.

Herein, we realize the direct synthesis of uniformly aligned VGs through a catalyst-free thermal CVD method for the first time. The successful fabrication of VGs in thermal CVD without the aid of plasma offers new insight for intrinsic vertical graphene growth mechanism. Furthermore, systematical experimental and theoretical investigations have been carried out to elucidate the formation mechanism of VGs by this novel technique. Based on the experimental observations and energy analysis, it's found that the concentration of active carbon species in CVD system exerts significant impact on the growth mode of graphene. Simply, by tuning the carbon precursor flow rate and reaction time during the CVD process, precise control of the growth dynamics can be achieved, leading to well-controlled morphology of the obtained carbon material, such as 2D graphene film or 3D vertical graphene sheets. Owing to the intrinsic driving force of the self-assembly mechanism, this strategy also shows specific substrate-independent and carbon precursor-independent superiority, offering a facile and versatile route for VGs fabrication with diverse substrates and precursors. Combining with the intrinsic excellent electrical conductivity of graphene itself and this unique structure of VGs, the as-prepared VGs can act as an ideal candidate for field emitter. Field-emission measurements demonstrate that the obtained VGs acquire outstanding field-emission properties comparable to those prepared by PECVD.

2. Experimental section

2.1. Synthesis of VGs

The vertically-oriented graphene sheets were directly grown on various substrates by using either methane or ethanol as carbon feedstock in a conventional ambient pressure CVD apparatus. Among the four substrates, quartz, silicon, SiO_2/Si, and ZrO_2/Si, employed for graphene growth, 300 nm SiO_2/Si chips were obtained by thermal oxidation [34,35], and ZrO_2/Si chips were obtained by depositing precise thickness of metal oxide layer on Si wafer through atomic layer deposition (ALD) [36,37] as reported in literature. Before loading the substrates into a horizontal quartz tube inside a hot-wall quartz tube furnace, a thorough cleaning procedure with deionized water, acetone, and ethanol was successively executed to remove the inorganic and/or organic impurities on the surface of substrates. In the case of utilizing liquid ethanol as the carbon source, ethanol vapor was introduced into the chamber by passing hydrogen (H_2) gas through the liquid container to bubble ethanol solution. The amount of ethanol introduced into the chamber could be quantitatively tuned by controlling the flow rate of H_2 gas. Prior to VGs growth, the CVD system was pumped from ambient pressure to ~10 Pa and then purged with pure hydrogen (H_2) gas until reaching atmospheric pressure. This process was repeated for three times to assure that there was no air residue in the quartz tube before heating the furnace. Briefly, the whole CVD process could be described as follows. First, a certain kind of substrate was mounted to the central region of the quartz tube and heated from room temperature to 1130 °C in 50 min with 50 sccm H_2 and 50 sccm Ar as carrier gas. Second, the substrate was annealed for 20 min at 1130 °C, and then a certain flow rate of methane or ethanol vapor was brought into the chamber to initiate graphene growth. The growth mode, two-dimensional growth or three-dimensional growth, of graphene could be controlled by altering feedstock concentration and/or reaction time. Finally, at the end of the growth, the flow of CH_4 or H_2 (for ethanol-based growth case) was switched off, and the system cooled down to room temperature in about 30 min.

2.2. VGs characterization

The as-grown VGs samples were systematically characterized by SEM (Hitachi S-4800; operating at 15 kV), Raman spectroscopy (Renishaw Invia plus; excitation: 532 nm laser), AFM (NanoMan VS microscope; working at a tapping mode), XPS (ESCA Lab220I-XL spectrometer using an Al-K-α X-ray as the excitation source; base pressure about 3×10^{-9} mbar; binding energies referenced to the C 1s line at 284.8 eV), TEM (JEOL JEM-2100F; operating at 200 kV). All characterizations of VGs were directly conducted on the substrate except for TEM analysis. The VGs transfer process for TEM analysis was modified from the literature reported method [38]. Briefly speaking, the obtained VGs/SiO_2 samples were etched by a PMMA-assisted method in a 15.0 M NaOH aqueous solution for 1.0 h. After the SiO_2 was totally dissolved, VGs were transferred onto TEM grids for further characterization.

2.3. Field-emission measurements

The field-emission performances of the VGs were carried out with parallel electrodes by employing an ITO-coated glass as an anode and as-synthesized VGs with underlying graphene films as a cathode in a high vacuum chamber (5×10^{-5} Pa). The distance between the anode and cathode was kept at 150 μm. The direct voltage could be accurately adjusted in the range of 0–1100 V. At low applied fields and currents, the *J-E* behavior of the as-grown VGs can be closely described by the Fowler-Nordheim (F-N) Eq. (1) [39,40]:

$$J = \frac{A\beta^2 E^2}{\phi} \exp\left(\frac{-B\phi^{3/2}}{\beta E}\right) \quad (1)$$

where, J is the emission current density (A m^{-2}), E is the applied electric field (V m^{-1}), ϕ is the work function (eV) of graphene, and β is the electric field enhancement factor, A (1.57×10^{-10} A V^{-2} eV) and B (6.83×10^3 V m^{-1} $eV^{-3/2}$) are the constants related to the work function.

3. Results and discussion

Here, direct growth of VGs on various substrates was realized by a simple atmospheric CVD process at 1130 °C without any external template or catalyst. Several technologically important and

representative substrates, such as silicon (semiconductor), silicon oxide (insulator) and quartz (transparent substrate), were employed to conduct VGs growth. The schematic illustration of the VGs growth process through a template-free, catalyst-free and plasma-absent CVD method is presented in Fig. 1a. In this system, CH_4 gas with a flow rate typically from 7 to 14 sccm (standard cubic centimeter per minute) was introduced to the chamber to ensure direct VGs growth on the substrate under a constant carrier gas flow of 50 sccm H_2 and 50 sccm Ar. Fig. 1b and c demonstrate the scanning electron microscopy (SEM) images of the large area and high density of vertical-morphology graphene sheets, providing a good perspective of the densely exposed edges for the as-synthesized VGs with similar morphology with those produced by PECVD [10,14,30,41]. As shown in Fig. 1b, the distribution of the well-aligned vertical graphene sheets was remarkably uniform over the whole surface area of the substrate. The height of vertical graphene sheet was estimated to be about 200 nm from the 45° tilt side-view image (Fig. S1). In particular, Fig. 1c exhibits a loose and porous morphology of the obtained VGs, suggesting a well-parallel alignment between individual graphene sheets.

Furthermore, the morphology of VGs is revealed by using transmission electron microscopy (TEM). Fig. 1d shows the TEM image of high-density VGs, in which the vertical graphene sheets are observed as wrinkle-like. Cross-sectional views of the VGs in Fig. 1d and Figs. S2a–b show the vertical standing of graphene sheets on the substrate with transparent edges. High-resolution TEM (HR-TEM) images (Figs. S2c–d) displayed a knife-edge with a 4 nm thick base and a 1–3 nm thick sharp edge composed of perfect graphite structure, implying the VGs films are terminated with a thickness corresponding to few-layer graphene. The most unique features of the VGs are the high density of edge sites and defects. In order to confirm these two points, Raman spectrum was employed based on the fact that, the intensity ratio of D band to G band (I_D/I_G) could stand for the defect density to a certain degree [42]. The co-presence of the characteristic 2D peak of graphene and ultra-high intensity of defect-related D peak in the typical Raman spectrum indicated high disorder level of VGs (Fig. 1e). The sp^2-bonded carbon in the VGs is further confirmed by X-ray photoelectron spectroscopy (XPS) measurements (Fig. S3a). In the full XPS spectrum (Fig. S3b), no signal of metal ions was detected, which further proved the direct growth of VGs on substrates in the absence of any metal catalysts.

To shed light on the detailed growth process of VGs in thermal CVD, the evolution of VGs is monitored by varying the growth time. The detailed process of VGs formation by this template-free CVD method is schematically illustrated in Fig. 2a. At the beginning of growth stage, graphene flakes randomly nucleate on the surface of substrate and enlarge to form continuous film. Once the underlying buffer layer formed, initial planar graphene growth eventually alters to upward growth. As a result, the following carbon atoms from feedstock thermal cracking continuously incorporate into the open edges to make the unique vertical growth proceed. The atomic force microscopy (AFM) images in Fig. 2b–d corresponded to the different growth periods at 1, 2, and 6 h under a condition of CH_4/H_2/Ar flow rate of 8/50/50 sccm, respectively. AFM height images demonstrated that, with the reaction proceeding, the mode of graphene growth made a transition from isolated planar flakes to continuous thin film and finally to vertically-oriented sheets. Also, the corresponding SEM images at different duration time provided more evidences on the detailed growth process of VGs (Fig. 2e–g). More importantly, the unique spatial structure that VGs root in the preliminary 2D graphene film is further confirmed by the partially rolled VGs sample. The transition of the growth mode was directly demonstrated by the coexistence of 2D graphene film and 3D VGs in SEM image (Fig. S4). The difference in surface morphology between the upper vertical layer (Fig. S4a and left region of Fig. S4b) and the bottom 2D layer (right region of Fig. S4b) gave clear evidences on the special architecture of the obtained VGs in our system. The large amount of opening edges of VGs can be reflected by the defect-related D peak intensity. Thus, we calculated the I_D/I_G value at different growth times. As shown in Fig. S5, the defect density dropped over time due to the gradual enlargement of 2D graphene flakes and then increased remarkably after VGs formation, strongly suggesting the successive VGs evolution process.

In a thermal CVD system here, the growth of VGs indicates that the vertical alignment of graphene follows a mechanism without relevance to plasma. Contrast to the conventional 2D film growth even for an ultra-long duration up to 72 h by previously reported catalyst-free thermal CVD method [43], high-density 3D VGs are obtained in a short time here. In order to reveal the key points in

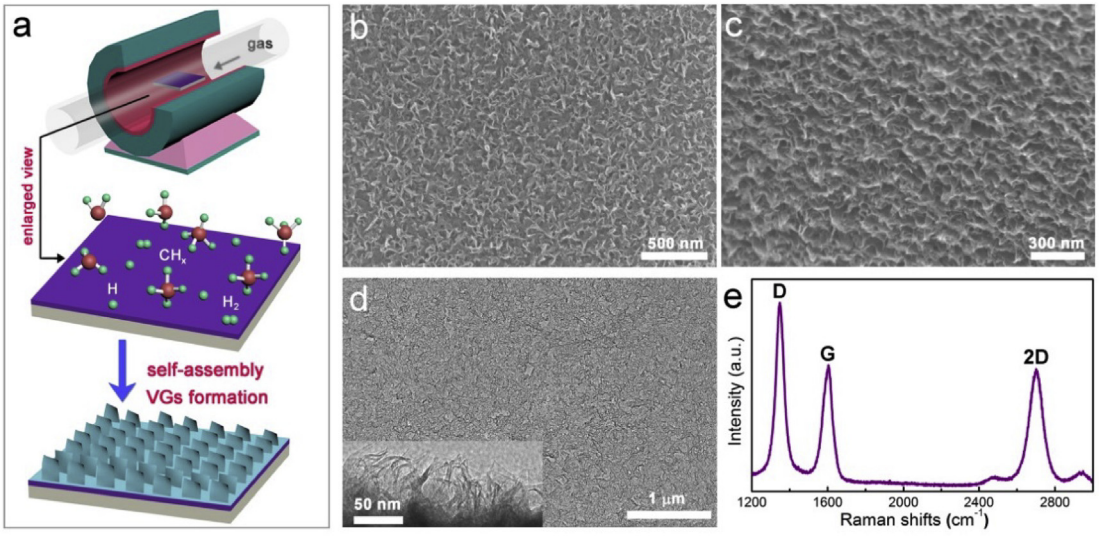

Fig. 1. Growth and characterizations of self-assembled VGs. (a) Schematic illustration of the template-free and catalyst-free CVD growth process of VGs. (b–c) Top view SEM images of as-grown VGs. (d) Wide-range TEM image of high-density VGs. Inset is the cross-sectional view. (e) Typical Raman spectrum of the as-grown VGs. The sample in (b–e) was prepared at 12 sccm CH_4, 50 sccm H_2 and 50 sccm Ar for 4 h. (A colour version of this figure can be viewed online.)

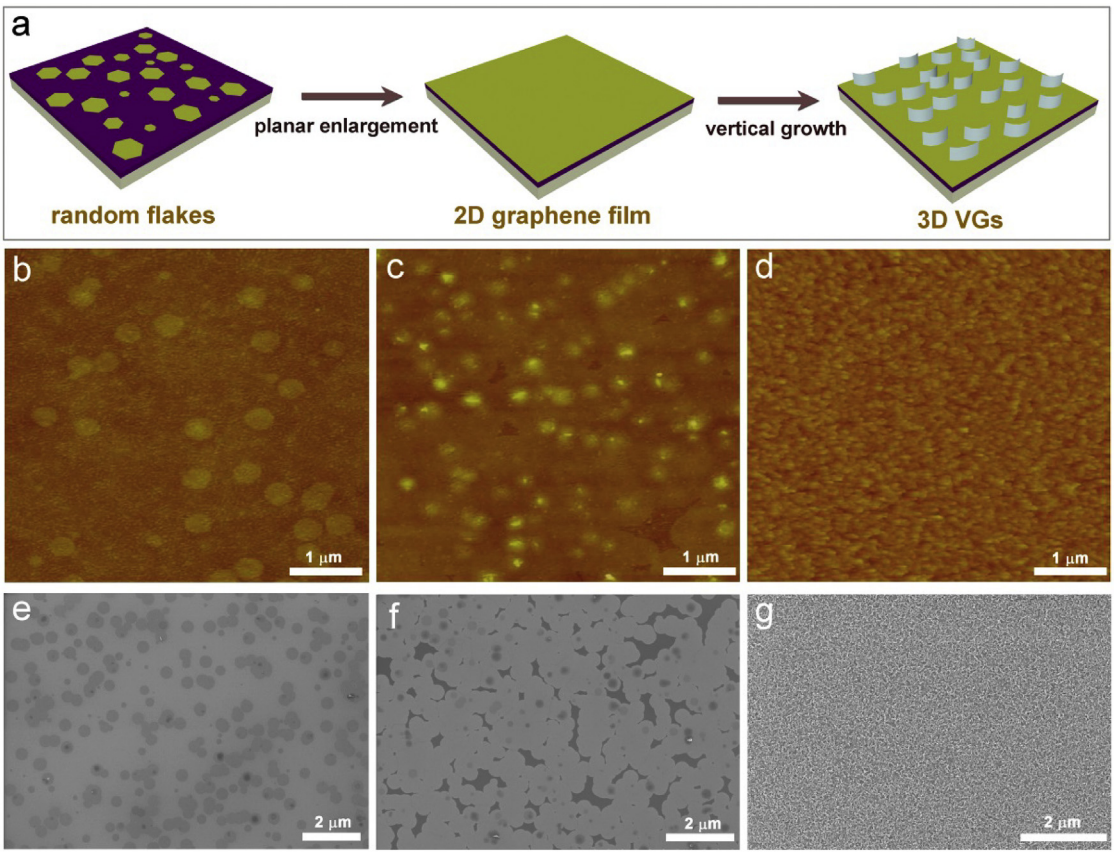

Fig. 2. Time-dependent evolution of the VGs growth. (a) Schematic illustration of the VGs growth at different time duration. (b–d) AFM images of graphene grown for 1, 2 and 6 h, respectively. (e–g) Corresponding SEM images of graphene samples in b-d. Conditions: 1130 °C under $CH_4/H_2/Ar$ flow rates of 8/50/50 sccm. (A colour version of this figure can be viewed online.)

determining the growth mode of graphene, we systematically performed control experiments under different conditions by tuning the flow rate of CH_4 gas and growth time while remaining temperature and flow rates of auxiliary gases unchanged. As shown in Fig. 3a, a few of individually separated regular hexagonal and/or circular graphene domains appeared under low CH_4 concentration (CH_4 flow rate below 7 sccm), consistent with the previously reported results [43–47]. Extending growth time just led to the enlargement of the domain size, the coverage area of graphene on substrates and the layer number of graphene film (Figs. S6a and b). Through conducting graphene growth at a larger CH_4 flow rate (10 sccm), we could find that high-density VGs were formed, presented in Fig. 3b. Further increasing the flow rate of CH_4 to 13 sccm, the CH_4 concentration is high enough to trigger three-dimensional graphene developing in a relatively short duration. Although the coverage of graphene was relatively low after 0.5 h of growth, considerable amounts of VGs had already emerged on the substrate (Fig. S6d). By prolonging growth duration, high-density and large-area VGs with underlying buffer layer were also obtained (Fig. S6e). Also, the planar graphene film and VGs obtained in Fig. S6b and Fig. S6e are confirmed by Raman spectra respectively in Fig. S6c and Fig. S6f. As shown in Fig. 3c, an ultra-high CH_4 flow rate, such as 15 sccm, led to amorphous carbon formation, resulting from the incomplete decomposition of CH_4. The corresponding Raman spectra in Fig. 3d–f well showed the dependence of the obtained morphology and structure of graphene on carbon precursor concentration. Thus, it demonstrates that the growth of VGs requires limited carbon concentration under a special CH_4 flow rate. In order to determine the critical value of CH_4 flow rate for achieving 3D graphene growth, a series of comprehensive experiments are performed and the detailed experimental results are listed in Table S1. We can find that, for achieving vertical graphene growth, a CH_4 flow rate between 7 and 14 sccm is necessary while keeping flow rates of other carrier gases constant in our system. As well, the graphene growth at 7 sccm CH_4 was provided in Fig. S7 to give an obvious transition from planar to vertical growth. Based on the above results, we claim that carbon precursor concentration, such as the flow rate of CH_4, is in charge of the growth mode of graphene.

The preference of vertical growth under special condition is supported by our detailed energy analysis. Under low CH_4 flow rate, the decomposition of carbon precursor matches well with the adsorption of carbon atom on active sites and the growth of graphene. Thus, the diffusion of carbon species to edge of graphene proceeds under a thermodynamic equilibrium condition and has enough time to reach the optional positions with minimum energy to form stable crystalline phases [48]. As a result, only 2D stacked nanometer- or micrometer-sized graphene flakes and films are obtained even after extraordinary long reaction duration [43]. While under a larger CH_4 flow rate, the concentration of carbon precursor is high enough to limit the effective diffusion of carbon species on substrate or graphene surface. In such cases, the graphene multi-nucleation and enlargement induced by the supersaturation of active carbon species concentration lead to the available surface of substrate shrinking into narrow channels. Then the reduction in fast-diffusion paths of carbon species along the surface makes the direct deposition of carbon to the graphene edges the main path of carbon addition. Thus, the edge reaction occurring on a fast time scale will lead to the vertical growth rather

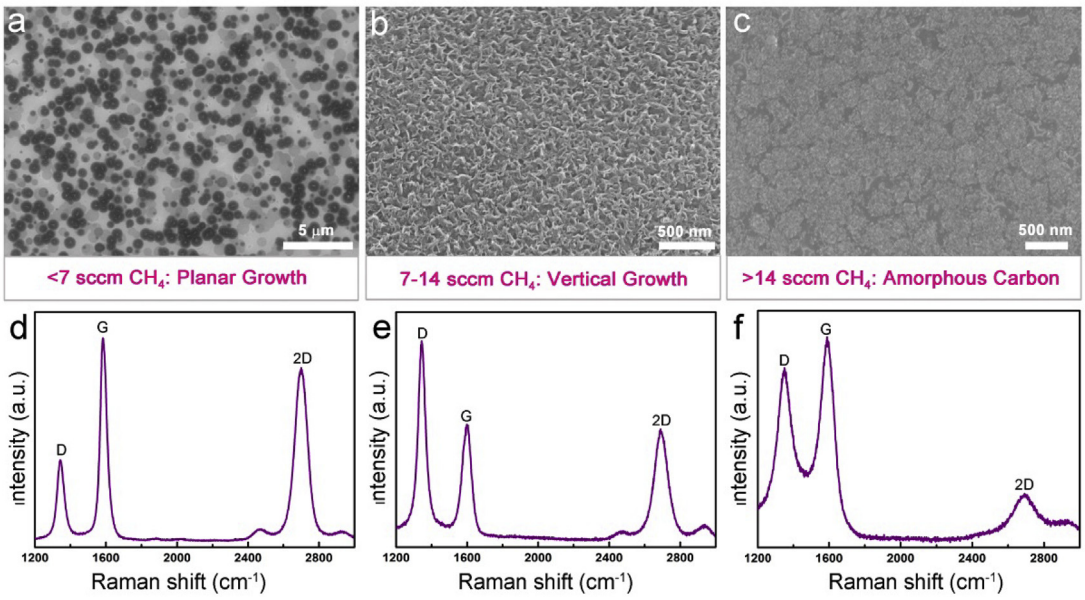

Fig. 3. Three typical growth modes of carbon materials in CVD growth depending on methane flow rate. (a) SEM image of the sample obtained under two-dimensional planar growth mode. The sample was prepared at 6 sccm CH_4, 50 sccm H_2 and 50 sccm Ar for 4 h. (b) SEM image of the sample obtained under three-dimensional vertical growth mode. The sample was prepared at 12 sccm CH_4, 50 sccm H_2 and 50 sccm Ar for 4 h. (c) SEM image of the sample obtained under amorphous carbon growth mode. The sample was prepared at 16 sccm CH_4, 50 sccm H_2 and 50 sccm Ar for 2 h. (d–f) Corresponding Raman spectra of the samples in a-c, respectively. (A colour version of this figure can be viewed online.)

than the boundary coalescence when two graphene islands approaching. In fact, this mechanism also explains why non-catalytic CVD techniques enhanced by plasma are prone to result in the growth of vertical graphene sheets [2,8,10,30,49]. Actually, due to the substantial quantity of carbon radicals released in the plasma, the transient concentration of carbon atom is high enough to result in an edge-reaction-dominated growth. The growth of 2D graphene by PECVD in previous works further demonstrates that the plasma is not the indispensible role for vertical graphene formation [50,51], but the carbon species concentration as established here.

As the adjacent graphene islands continue to grow in the edge-addition-dominated regime, a vertical or folded morphology may be considered as the one they evolve into eventually. To understand how the growth model is chosen during growth of VGs, we present an energy analysis of a vertical or folded graphene sheet merged by two layer graphene flakes on flat substrate (Fig. 4a–b). By assuming the two layers have the same excess length L, defined as the length of graphene that is not adhered to the substrate, we calculate their elastic and adhesion energies (see details in Supporting Information). Our energy analysis shows that if we define an excess length L for the length of graphene not adhered to the substrate, the vertically aligned morphology will be energetically more favorable for $L < L_c = 5.9$ nm (Fig. 4c). Beyond this critical value of excess length L_c, the folded morphology is lower in energy, and there is a significant energy barrier (7.4 eV/nm) between the vertical and folded configuration. The value of this barrier is calculated from the difference in energy for the configurations in Fig. 4a and b through Equations S1 and S5. In consequence, after the vertical graphene sheets nucleating and proceeding to grow upward, it is difficult for them to bend into the folded morphology without strong external perturbation. This preference is much more obvious for multilayers as the bending stiffness κ increases significantly with the number of layers N, that is, $\kappa \sim N^3$ [52]. In order to provide a clearer view of the transition process, we perform the structure characterization of vertical graphene sheets at their early stage. As stated former, the vertical growth is induced by two approaching graphene islands, which is definitely confirmed by the AFM and TEM images in Fig. 4d–f. This observation is totally different from the graphene growth under low CH_4 flow rate that two adjacent graphene islands with mismatch in their in-plane lattice orientation prefer to form a continuous layer with grain boundary (Fig. S8). Combined with the experimental evidence we have discussed, the results from energy analysis clearly and directly demonstrated the detailed evolution process of VGs in this plasma-absent CVD system. Further, the three procedures involved in the growth evolution (Fig. 2a) are quite similar with those VGs growth in a PECVD system, as well as the similar morphology observed [53]. These evidences indicated that the VGs growth in this system might follow the same mechanism as discussed above, *i.e.* the high carbon species concentration determines the 3D VGs growth mode.

We have clearly elucidated the evolution process and formation mechanism of VGs, while another feature of VGs should be taken into account: the density and height of the expected VGs, which greatly affect the application of VGs in a lot of fields. We find that the controllable VGs formation can readily be realized by tuning the growth time under a given condition. Large-area VGs were successively prepared under varied growth time from 2 to 6 h at CH_4/H_2/Ar flow rate of 10/50/50 sccm (Fig. 5a–c). It demonstrated that the density of vertical graphene sheets gradually increased along with growth proceeding. The corresponding contact angles of water on the VGs obtained at 2 h, 4 h and 6 h increase from 69.3 to 114.1°, which could also provide evidences on the increased density of the as-synthesized VGs, as shown in the inset panels of Fig. 5a–c. A more systematical correlation between contact angles of water on the VGs and density of vertical graphene sheets was provided in Fig. S9. In addition to the high controllability on VGs density, this gradual growth process as well allows it possible to tune the height of VGs. An evolutionary cross-sectional SEM characterization of VGs as a function of growth time was conducted for comparison (Fig. 5d–f). Along with extending growth period, it was obvious

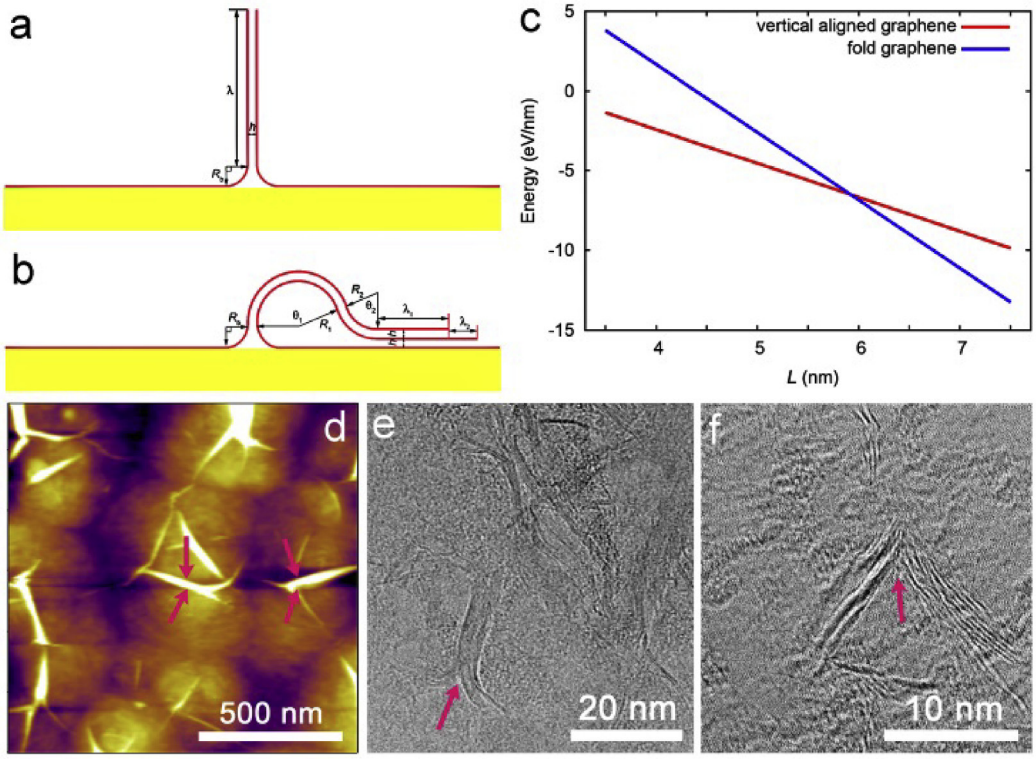

Fig. 4. Energy analysis and formation mechanism of VGs growth. (a–b) Formation of vertical graphene multilayers (a) and folded graphene layers (b). For simplicity, the underlying graphene buffer layers are ignored in the schematic illustration. (c) Comparison between the total energy of vertical and folded graphene, as a function of the excess length *L*. (d) AFM image of low-density VGs. Obviously, the vertical graphene sheets are induced by the two or more individual approached graphene flakes, as marked by the red arrows. (e–f) HRTEM images of VGs, indicating that the vertical sheet roots in two adjacent graphene sheets. (A colour version of this figure can be viewed online.)

that the average height of vertical graphene sheets increased successively. The corresponding 3D AFM surface plots and height profiles (Fig. S10) further unambiguously confirmed the increase of VGs height and density. The simultaneous growth in VGs density and height shed lights on the formation process that once nucleation sites for vertical growth developed, following carbon supply could facilitate growth along the vertical graphene sheet and hasten more nucleation sites. However further extremely prolonging growth duration not led to the increase of height of vertical graphene sheets, but yielded aggregated cluster-like structure with almost unchanged height (Fig. S11). By optimizing the growth process, direct control over the density and height of vertical graphene sheets can be ultimately realized, suggesting the high controllability and versatility of this template-free CVD method.

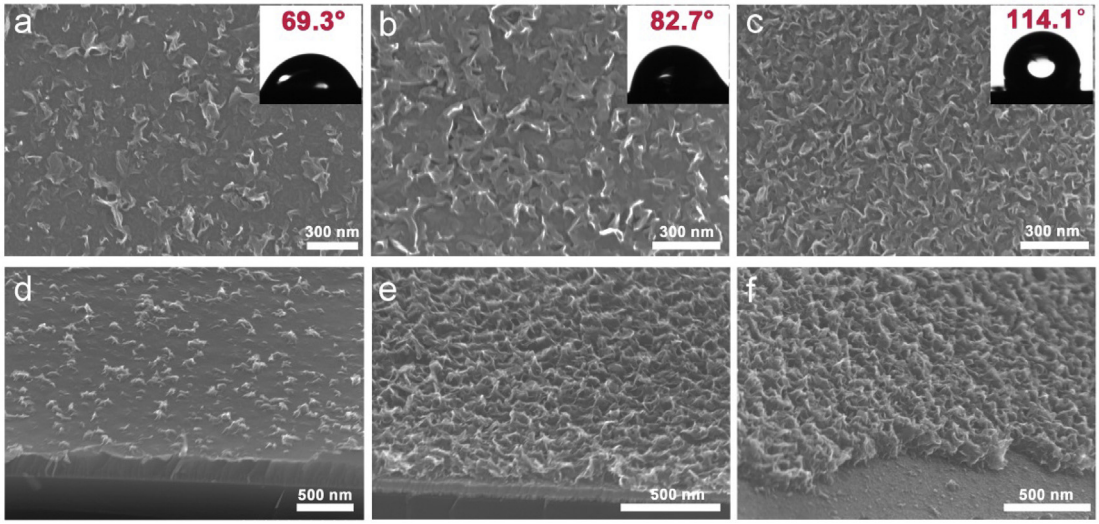

Fig. 5. Density- and height-engineering of VGs. (a–c) SEM images of VGs grown for 2, 4 and 6 h, respectively. Insets are corresponding static water contact angle. Conditions: 1130 °C under CH_4/H_2/Ar flow rates of 10/50/50 sccm. (d–f) Corresponding cross-sectional SEM images of VGs in a-c, respectively. (A colour version of this figure can be viewed online.)

Another prominent advantage of this approach is that it can be applied to various substrates and feedstock of carbon sources, enabling the wide versatility and scalability of this method. In order to gain an in-depth understanding on this point, we carried out graphene growth on quartz, Si, and ZrO_2 by using CH_4 as the carbon source. Under the same conditions (1130 °C, 8 sccm CH_4, 50 sccm H_2 and 50 sccm Ar at ambient pressure), high-density and large-area VGs were obtained after 6 h of growth on whatever kinds of substrates (Figs. S12a–c). The qualities of the obtained VGs were as good as that synthesized on SiO_2 (Fig. 1b). Furthermore, it was amazing to find that VGs growth could also be achieved by using liquid carbon precursor. As shown in Fig. S12d, high quality of VGs was also obtained by employing ethanol as a carbon source. The effect of ethanol content, quantitatively tuned by controlling the flow rate of H_2 carrier gas, in the system on VGs formation had been found to give a similar influence with that of CH_4, see detailed results in Table S2. Therefore, VGs with similar quality and density using various substrates and feedstock indicated that this approach provided a reliable and controllable strategy to achieve high yields of VGs preparation for practical applications.

To further evaluate the property of as-prepared VGs by our template-free and catalyst-free thermal CVD method, the electron-field-emission performances were investigated by employing an indium tin oxide (ITO)-coated glass as anode and VGs with underlying graphene films as cathode in a high vacuum chamber. The distance between the anode and cathode was 150 μm. Fig. 6a shows the typical field emission current density (J) as a function of applied electric field (E) for an as-grown VGs sample obtained at 12 sccm CH_4, 50 sccm H_2, and 50 sccm Ar for 4 h of growth. The inset panel in Fig. 6a presents the emission pattern for the VGs emitter collected at an applied field of 2.67 V/μm. The turn-on field (E_{on}) is defined as the electric field for emitting a current density of 10 μA/cm^2, while the threshold field (E_{thres}) is the electric field for reaching a current density of 1 mA/cm^2, which is sufficient to achieve panel display. Strikingly, an ultra-low turn-on field (1.07 V/μm) and threshold field (1.65 V/μm) were observed, presenting an excellent field emission property of the obtained VGs. We compare the field-emission performances of our VGs with the reported results, and it can be found that performances obtained here outperform most of the reported field-emission properties of graphene materials, see details in Table S3. Fowler-Nordheim (F-N) equation has been widely used to investigate the electron-emission behavior of various nanostructure materials. The good linearity of F-N plots means that the cathode material agrees well with this model. Then, we plotted $\ln(J/E^2)$ as a function of $1/E$, which yielded a fitted line shape with a good agreement with F-N equation (Fig. 6b). Due to the unique geometry of the emitter and its surface morphology, a high field-enhancement factor by enhanced local electric field is expected. Assuming the work function of graphene as that of graphite (~5 eV) [54], the field-enhancement factor (β) of the as-grown VGs was estimated to be 2.55×10^3 from the linear F-N slope, which is higher than previously reported values [55,56]. The high stability of the field emission performance was also investigated by conducting measurement for 1800 s (sampling time interval is 200 ms) with negligible current-density degradation (Fig. 6c). To reveal the enhancement mechanism in the performance of our VGs-based field emitters, we schematically elucidated the relation between the density of standing graphene sheets and the field emission performance of the VGs samples (Fig. 6d). The negative correlation between turn-on/threshold fields and VGs density indicated that the field emission performance of VGs can be well controlled and further improved by increasing VGs density. Generally, a strongly local electric filed forms at the tip region of vertical graphene sheet when it is subjected to an external electric

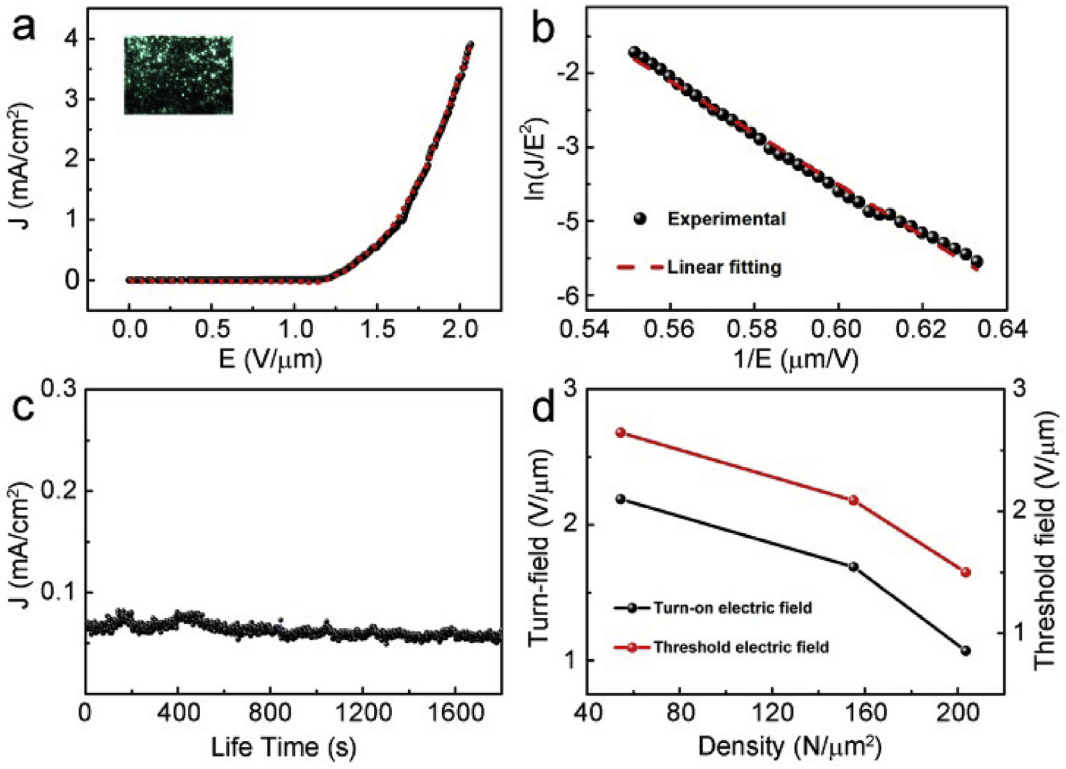

Fig. 6. Field-emission properties of the as-grown VGs. (a) Typical plot of the electron-emission current density (J) as a function of applied electric field (E) for the VGs. Inset: emission pattern for the VGs emitter collected at an applied field of 2.67 V/μm. (b) Corresponding F-N plot. (c) Current-emission stability of the VGs at room temperature within 1800 s. (d) Turn-on electric field and threshold electric field as a function of VGs density. (A colour version of this figure can be viewed online.)

field. Thus, the high length/diameter ratio and extremely abundant edge-sites of the high-density VGs can effectively reduce the acquired external field for field emission. Here, we attribute such excellent field-emission performance of VGs to its special architecture and 2D-3D graphene framework. With densely exposed sharp edges and highly intrinsic electrical conductivity, such unique architecture can build up an excellent mechanical and electrical contact between the current collector and active materials. These features can facilitate electron transport during the electron emission process, implementing field emitters with a low turn-on filed and a high field enhancement factor.

4. Conclusions

In summary, we have successfully and elaborately demonstrated a novel strategy for facile synthesis of large-area and high-density 3D VGs on various substrates via a thermal CVD method. Systematic investigations on evolution process indicate that the key point for VGs formation is the carbon precursor concentration in the CVD process. The formation mechanism of VGs growth in CVD is elucidated by detailed energy analysis as well. Importantly, through simply tuning carbon precursor flow rate and growth time, controllability on the density and height of the obtained VGs can be easily achieved. Furthermore, benefiting from the unique structure and special properties of VGs, such as large quantity of atomically fresh edges and outstanding electrical conductivity, the as-grown VGs exhibit excellent field-emission performance with a low turn-on electric field of 1.07 V/μm, a low threshold field of 1.65 V/μm, and good emission stability. Based on the mentioned above, we believe that this technique will be a good alternative for large-scale VGs preparation and widespread practical applications.

Acknowledgments

We acknowledge the financial support from the National Natural Science Foundation of China (61390502), the National Major State Basic Research Development Program (2013CB933403 and 2013CBA01602), and the Strategic Priority Research Program of the Chinese Academy of Sciences (XDB 12030100).

Appendix A. Supplementary data

Supplementary data related to this article can be found at http://dx.doi.org/10.1016/j.carbon.2017.05.074.

References

[1] J. Chen, B. Zheng, G. Lu, Vertically-oriented Graphene, Springer International Publishing, 2015.
[2] Y.H. Wu, P.W. Qiao, T.C. Chong, Z.X. Shen, Carbon nanowalls grown by microwave plasma enhanced chemical vapor deposition, Adv. Mater. 14 (1) (2002) 64–67.
[3] J.R. Miller, R.A. Outlaw, B.C. Holloway, Graphene double-layer capacitor with ac line-filtering performance, Science 329 (5999) (2010) 1637–1639.
[4] Z. Bo, S. Mao, Z.J. Han, K.F. Cen, J.H. Chen, K. Ostrikov, Emerging energy and environmental applications of vertically-oriented graphenes, Chem. Soc. Rev. 44 (8) (2015) 2108–2121.
[5] A. McLeod, S. Kumar, K.C. Vernon, K. Ostrikov, Vertical graphene nanosheets coated with gold nanoparticle arrays: effect of interparticle spacing on optical response, J. Nanomater. 2015 (2015) 230987.
[6] D.H. Seo, A.E. Rider, S. Kumar, L.K. Randeniya, K. Ostrikou, Vertical graphene gas- and bio-sensors via catalyst-free, reactive plasma reforming of natural honey, Carbon 60 (2013) 221–228.
[7] P. Slobodian, U. Cvelbar, P. Riha, R. Olejnik, J. Matyas, G. Filipic, et al., High sensitivity of a carbon nanowall-based sensor for detection of organic vapours, RSC Adv. 5 (110) (2015) 90515–90520.
[8] N.G. Shang, P. Papakonstantinou, M. McMullan, M. Chu, A. Stamboulis, A. Potenza, et al., Catalyst-free efficient growth, orientation and biosensing properties of multilayer graphene nanoflake films with sharp edge planes, Adv. Funct. Mater. 18 (21) (2008) 3506–3514.
[9] M.Z. Cai, R.A. Outlaw, R.A. Quinlan, D. Premathilake, S.M. Butler, J.R. Miller, Fast response, vertically oriented graphene nanosheet electric double layer capacitors synthesized from C2H2, ACS Nano 8 (6) (2014) 5873–5882.
[10] Z. Bo, W.G. Zhu, W. Ma, Z.H. Wen, X.R. Shuai, J.H. Chen, et al., Vertically oriented graphene bridging active-layer/current-collector interface for ultrahigh rate supercapacitors, Adv. Mater. 25 (40) (2013) 5799–5806.
[11] C. Zhu, P. Yang, D. Chao, X. Wang, X. Zhang, S. Chen, et al., All metal nitrides solid-state asymmetric supercapacitors, Adv. Mater. 27 (31) (2015) 4566–4571.
[12] D.H. Seo, S. Yick, Z.J. Han, J.H. Fang, K. Ostrikov, Synergistic fusion of vertical graphene nanosheets and carbon nanotubes for high-performance supercapacitor electrodes, ChemSusChem 7 (8) (2014) 2317–2324.
[13] T.C. Hung, C.F. Chen, W.T. Whang, Deposition of carbon nanowall flowers on two-dimensional sheet for electrochemical capacitor application, Electrochem. Solid State Lett. 12 (6) (2009) K41–K44.
[14] J.L. Qi, X. Wang, J.H. Lin, F. Zhang, J.C. Feng, W.D. Fei, A high-performance supercapacitor of vertically-oriented few-layered graphene with high-density defects, Nanoscale 7 (8) (2015) 3675–3682.
[15] B. Ouyang, Y.Q. Zhang, Z. Zhang, H.J. Fan, R.S. Rawat, Green synthesis of vertical graphene nanosheets and their application in high-performance supercapacitors, RSC Adv. 6 (28) (2016) 23968–23973.
[16] X. Cao, Z. Yin, H. Zhang, Three-dimensional graphene materials: preparation, structures and application in supercapacitors, Energy Environ. Sci. 7 (6) (2014) 1850–1865.
[17] Y. Zhang, J.L. Du, S. Tang, P. Liu, S.Z. Deng, J. Chen, et al., Optimize the field emission character of a vertical few-layer graphene sheet by manipulating the morphology, Nanotechnology 23 (1) (2012) 015202.
[18] J.L. Liu, B.Q. Zeng, X.R. Wang, W.Z. Wang, H.L. Shi, One-step growth of vertical graphene sheets on carbon nanotubes and their field emission properties, Appl. Phys. Lett. 103 (5) (2013) 053105.
[19] C.Y. Cheng, M. Nakashima, K. Teii, Low threshold field emission from nanocrystalline diamond/carbon nanowall composite films, Diam. Relat. Mater. 27–28 (2012) 40–44.
[20] V. Krivchenko, P. Shevnin, A. Pilevsky, A. Egorov, N. Suetin, V. Sen, et al., Influence of the growth temperature on structural and electron field emission properties of carbon nanowall/nanotube films synthesized by catalyst-free PECVD, J. Mater. Chem. 22 (32) (2012) 16458–16464.
[21] E. Stratakis, R. Giorgi, M. Barberoglou, T. Dikonimos, E. Salernitano, N. Lisi, et al., Three-dimensional carbon nanowall field emission arrays, Appl. Phys. Lett. 96 (4) (2010) 043110.
[22] K. Teii, M. Nakashima, Synthesis and field emission properties of nanocrystalline diamond/carbon nanowall composite films, Appl. Phys. Lett. 96 (2) (2010) 023112.
[23] L.L. Jiang, T.Z. Yang, F. Liu, J. Dong, Z.H. Yao, C.M. Shen, et al., Controlled synthesis of large-scale, uniform, vertically standing graphene for high-performance field emitters, Adv. Mater. 25 (2) (2013) 250–255.
[24] Y. Wang, B. Chen, D.H. Seo, Z.J. Han, J.I. Wong, K. Ostrikov, et al., MoS2-coated vertical graphene nanosheet for high-performance rechargeable lithium-ion batteries and hydrogen production, NPG Asia Mater. 8 (2016) e268.
[25] C.X. Zhang, J. Hu, X.K. Wang, X.D. Zhang, H. Toyoda, M. Nagatsu, et al., High performance of carbon nanowall supported Pt catalyst for methanol electrooxidation, Carbon 50 (10) (2012) 3731–3738.
[26] A.T.H. Chuang, J. Robertson, B.O. Boskovic, K.K.K. Koziol, Three-dimensional carbon nanowall structures, Appl. Phys. Lett. 90 (12) (2007) 123107.
[27] I. Levchenko, K. Ostrikov, A.E. Rider, E. Tam, S.V. Vladimirov, S. Xu, Growth kinetics of carbon nanowall-like structures in low-temperature plasmas, Phys. Plasmas 14 (6) (2007) 063502.
[28] D. Premathilake, R.A. Outlaw, S.G. Parler, S.M. Butler, J.R. Miller, Electric double layer capacitors for ac filtering made from vertically oriented graphene nanosheets on aluminum, Carbon 111 (2017) 231–237.
[29] Y. Ma, H. Jang, S. Kim, C. Pang, H. Chae, Copper-assisted direct growth of vertical graphene nanosheets on glass substrates by low-temperature plasma-enhanced chemical vapour deposition process, Nanoscale Res. Lett. 10 (2015) 308.
[30] D.H. Seo, A.E. Rider, Z.J. Han, S. Kumar, K. Ostrikov, Plasma break-down and rebuild: same functional vertical graphenes from diverse natural precursors, Adv. Mater. 25 (39) (2013) 5638–5642.
[31] E. Sandoz-Rosado, W. Page, D. O'Brien, J. Przepioski, D. Mo, B. Wang, et al., Vertical graphene by plasma-enhanced chemical vapor deposition: correlation of plasma conditions and growth characteristics, J. Mater. Res. 29 (3) (2014) 417–425.
[32] J. Zhao, M. Shaygan, J. Eckert, M. Meyyappan, M.H. Rummeli, A growth mechanism for free-standing vertical graphene, Nano Lett. 14 (6) (2014) 3064–3071.
[33] Z. Bo, K.H. Yu, G.H. Lu, P.X. Wang, S. Mao, J.H. Chen, Understanding growth of carbon nanowalls at atmospheric pressure using normal glow discharge plasma-enhanced chemical vapor deposition, Carbon 49 (6) (2011) 1849–1858.
[34] A.E. Pap, K. Kordás, T.F. George, S. Leppävuori, Thermal oxidation of porous silicon: study on reaction kinetics, J. Phys. Chem. B 108 (34) (2004) 12744–12747.
[35] K.L. Jarvis, T.J. Barnes, C.A. Prestidge, Aqueous and thermal oxidation of porous silicon microparticles: implications on molecular interactions, Langmuir 24 (24) (2008) 14222–14226.
[36] J.R. Avila, E.J. DeMarco, J.D. Emery, O.K. Farha, M.J. Pellin, J.T. Hupp, et al., Real-

time observation of atomic layer deposition inhibition: metal oxide growth on self-assembled alkanethiols, ACS Appl. Mat. Interfaces 6 (15) (2014) 11891–11898.
[37] F. Li, X. Yao, Z. Wang, W. Xing, W. Jin, J. Huang, et al., Highly porous metal oxide networks of interconnected nanotubes by atomic layer deposition, Nano Lett. 12 (9) (2012) 5033–5038.
[38] H. Kim, I. Song, C. Park, M. Son, M. Hong, Y. Kim, et al., Copper-vapor-assisted chemical vapor deposition for high-quality and metal-free single-layer graphene on amorphous SiO2 substrate, ACS Nano 7 (8) (2013) 6575–6582.
[39] A.A. Al-Tabbakh, M.A. More, D.S. Joag, I.S. Mulla, V.K. Pillai, The Fowler–Nordheim plot behavior and mechanism of field electron emission from ZnO tetrapod structures, ACS Nano 4 (10) (2010) 5585–5590.
[40] L. Wu, H. Duan, P. Bai, M. Bosman, J.K.W. Yang, E. Li, Fowler–Nordheim tunneling induced charge transfer plasmons between nearly touching nanoparticles, ACS Nano 7 (1) (2013) 707–716.
[41] R.L. Liu, Y.Q. Chi, L. Fang, Z.S. Tang, X. Yi, Synthesis of carbon nanowall by plasma-enhanced chemical vapor deposition method, J. Nanosci. Nanotechnol. 14 (2) (2014) 1647–1657.
[42] J.X. Wu, H. Xu, J. Zhang, Raman spectroscopy of graphene, Acta Chim. Sin. 72 (2014) 301–318.
[43] J. Chen, Y. Guo, L. Jiang, Z. Xu, L. Huang, Y. Xue, et al., Near-equilibrium chemical vapor deposition of high-quality single-crystal graphene directly on various dielectric substrates, Adv. Mater. 26 (9) (2014) 1348–1353.
[44] J. Chen, Y. Wen, Y. Guo, B. Wu, L. Huang, Y. Xue, et al., Oxygen-aided synthesis of polycrystalline graphene on silicon dioxide substrates, J. Am. Chem. Soc. 133 (44) (2011) 17548–17551.
[45] H. Wang, G. Yu, Direct CVD graphene growth on semiconductors and dielectrics for transfer-free device fabrication, Adv. Mater. 28 (25) (2016) 4956–4975.
[46] J.Y. Sun, T. Gao, X.J. Song, Y.F. Zhao, Y.W. Lin, H.C. Wang, et al., Direct growth of high-quality graphene on high-kappa dielectric $SrTiO_3$ substrates, J. Am. Chem. Soc. 136 (18) (2014) 6574–6577.
[47] J.S. Chen, B. Wu, Y.Q. Liu, Synthesis of graphene on dielectric substrates, Acta Chim. Sin. 72 (2014) 359–366.
[48] M.-Q. Zeng, T. Zhang, L.-F. Tan, L. Fu, Liquid metal catalyst: philosopher's stone of two-dimensional materials, Acta Phys. -Chim. Sin. 33 (3) (2017) 464–475.
[49] D.H. Seo, Z.J. Han, S. Kumar, K. Ostrikov, Structure-controlled, vertical graphene-based, binder-free electrodes from plasma-reformed butter enhance supercapacitor performance, Adv. Energy Mater. 3 (10) (2013) 1316–1323.
[50] D.C. Wei, Y.H. Lu, C. Han, T.C. Niu, W. Chen, A.T.S. Wee, Critical crystal growth of graphene on dielectric substrates at low temperature for electronic devices, Angew. Chem. Int. Ed. 52 (52) (2013) 14121–14126.
[51] L.C. Zhang, Z.W. Shi, Y. Wang, R. Yang, D.X. Shi, G.Y. Zhang, Catalyst-free growth of nanographene films on various substrates, Nano Res. 4 (3) (2011) 315–321.
[52] E. Gao, Z. Xu, Thin-shell thickness of two-dimensional materials, J. Appl. Mech. 82 (12) (2015) 121012.
[53] Z. Bo, Y. Yang, J. Chen, K. Yu, J. Yan, K. Cen, Plasma-enhanced chemical vapor deposition synthesis of vertically oriented graphene nanosheets, Nanoscale 5 (12) (2013) 5180–5204.
[54] G. Giovannetti, P.A. Khomyakov, G. Brocks, V.M. Karpan, J. van den Brink, P.J. Kelly, Doping graphene with metal contacts, Phys. Rev. Lett. 101 (2) (2008) 026803.
[55] F. Liu, J. Tian, L. Bao, T. Yang, C. Shen, X. Lai, et al., Fabrication of vertically aligned single-crystalline boron nanowire arrays and investigation of their field-emission behavior, Adv. Mater. 20 (13) (2008) 2609–2615.
[56] W.-C. Yen, H. Medina, C.-W. Hsu, Y.-L. Chueh, Conformal graphene coating on high-aspect ratio Si nanorod arrays by a vapor assisted method for field emitter, RSC Adv. 4 (51) (2014) 27106–27111.

Supporting Information

Facile growth of vertically-aligned graphene nanosheets via thermal CVD: the experimental and theoretical investigations

Huaping Wang[a,b], Enlai Gao[c], Peng Liu[d], Duanliang Zhou[d], Dechao Geng[a,b], Xudong Xue[a,e], Liping Wang[e], Kaili Jiang[d,*], Zhiping Xu [c,*], Gui Yu [a,b,*]

[a] Beijing National Laboratory for Molecular Sciences, Institute of Chemistry, Chinese Academy of Sciences, Beijing 100190, P. R. China

[b] University of Chinese Academy of Sciences, Beijing 100049, P. R. China

[c] Applied Mechanics Laboratory, Department of Engineering Mechanics and Center for Nano and Micro Mechanics, Tsinghua University, Beijing 100084, P. R. China

[d] Department of Physics & Tsinghua-Foxconn Nanotechnology Research Center, Tsinghua University, Beijing 100084, P. R. China

[e] School of Materials Science and Engineering, University of Science and Technology Beijing, Beijing 100083, P. R. China

A Table of Contents

1. Details of the energy analysis

The total energy of vertical graphene sheet on flat substrate shown in Figure 4a, including the elastic bending energy in graphene, adhesion energy between graphene, adhesion between graphene and substrate, is

$$E_v = \pi\kappa/2R_b - \gamma_G\lambda + \gamma_{G/SiO2}(2R_b + h) \quad \text{(S1)}$$

Here κ is the bending stiffness of graphene, γ_G is van der Waals adhesion energy between graphene, and the excess length L of graphene is

$$L = \pi R_b/2 + \lambda - (R_b + h/2) \quad \text{(S2)}$$

R_b, λ, and h are the geometrical parameters illustrated in Figure 4a. We choose parameters κ = 1.4 eV, h = 3.4 Å, γ_G= 0.341 J/m^2 and $\gamma_{G/SiO2}$ = 0.229 J/m^2.[1,2]

By minimizing E_v with R_b as the parameter, we can find the value of R_b in Eq. S1 in the elastic equilibrium as

$$\frac{\partial E_v}{\partial R_b} = 0 \quad \text{(S3)}$$

$$R_b = \sqrt{\frac{\kappa\pi}{2[\gamma_G(\pi/2-1) + 2\gamma_{G/SiO_2}]}} \quad \text{(S4)}$$

Similarly, we can estimate the energy of the folded graphene bilayer on flat substrates in Figure 4b as

$$\begin{aligned} E_f &= \frac{\kappa}{2}\left(\frac{\pi}{R_b} + \frac{\theta_1}{R_1} + \frac{\theta_1}{R_1+h} + \frac{\theta_2}{R_2} + \frac{\theta_2}{R_2+h}\right) \\ &-\gamma_G\left[\left(R_1 + \frac{h}{2}\right)\theta_1 + \left(R_2 + \frac{h}{2}\right)\theta_2 + 2\lambda_1 + \lambda_2\right] + \gamma_{G/SiO_2}(2R_b + h) \end{aligned} \quad \text{(S5)}$$

The excess length of graphene here is

$$\begin{aligned} L &= \frac{\pi}{2}R_b + (R_1 + h)\theta_1 + R_2\theta_2 + \lambda_1 - \left(R_b + \frac{h}{2}\right) \\ &= \frac{\pi}{2}R_b + R_1\theta_1 + (R_2 + h)\theta_2 + \lambda_1 + \lambda_2 - \left(R_b + \frac{h}{2}\right) \end{aligned} \quad \text{(S6)}$$

There are three parameters R_b, R_1, θ_1 for a fixed excess length L, which could be solved by minimizing E_f with geometrical constraints on the angles and radii,

$$\theta_1 - \theta_2 = \pi/2 \quad \text{(S7)}$$

$$R_1\sin\theta_1 + R_b = h + (R_2 + h)(1 - \cos\theta_2) \quad \text{(S8)}$$

$$\lambda_2 = (\theta_1 - \theta_2)h = \pi h/2 \quad \text{(S9)}$$

By numerically minimizing the energies for vertically aligned and folded graphene bilayers (Eqs. S1 and S5), we find R_b = 0.73 nm for the VGs and R_b = 0.46 nm, θ_1 = 2.28 and R_1 = 0.50 nm for folded graphene. The total energies are summarized in Figure 4c as a function of the excess length L.

2. Supporting Figures

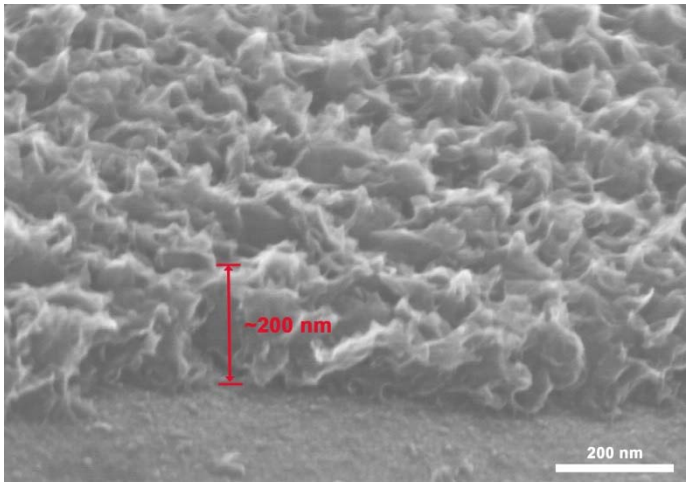

Figure S1. Height estimation from 45 degree tilt SEM images of VGs sample in Figure 1c.

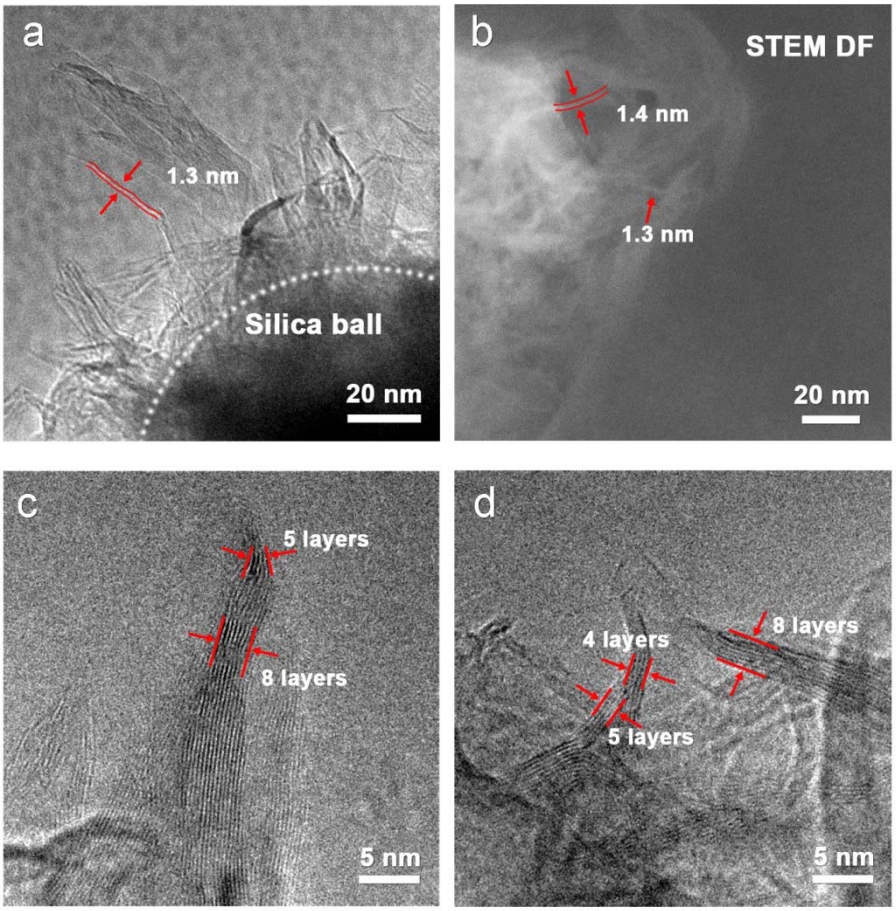

Figure S2. Thickness and layer number characterizations of the vertical graphene sheet in as-grown VGs. For TEM characterization, due to the cross-sectional TEM image can provide a clear view of sheet thickness, we prepared VGs on silica micro-balls and then transferred to TEM grids by etching the silica micro-balls. (a) Cross-sectional TEM views of VGs transferred from silica micro-balls. The residual silica ball that has not been etched fully is illustrated with the dotted lines. (b) TEM dark field image of VGs transferred from SiO_2/Si substrates. (c-d) High-resolution TEM images of VGs transferred from silica micro-balls.

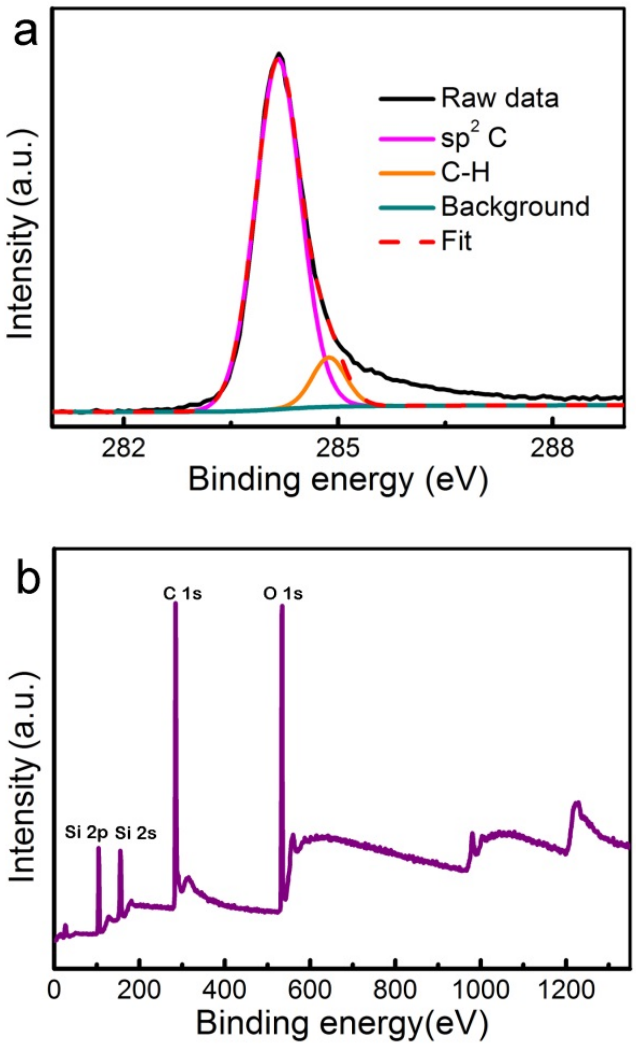

Figure S3. XPS analysis of the as-synthesized VGs on a SiO_2/Si substrate. (a) XPS C1s core-level spectrum of VGs. In the XPS C1s core-level spectrum, two peaks centered at binding energies of 284.2 and 284.9 eV were assigned to the sp^2 and sp^3 carbon content, which originated from the basal plane and opening edge of VGs, respectively. (b) Full XPS spectrum of the obtained VGs sample. In the spectrum, no signal of metal ions is observed, which demonstrates the absence of any co-catalyst for VGs formation.

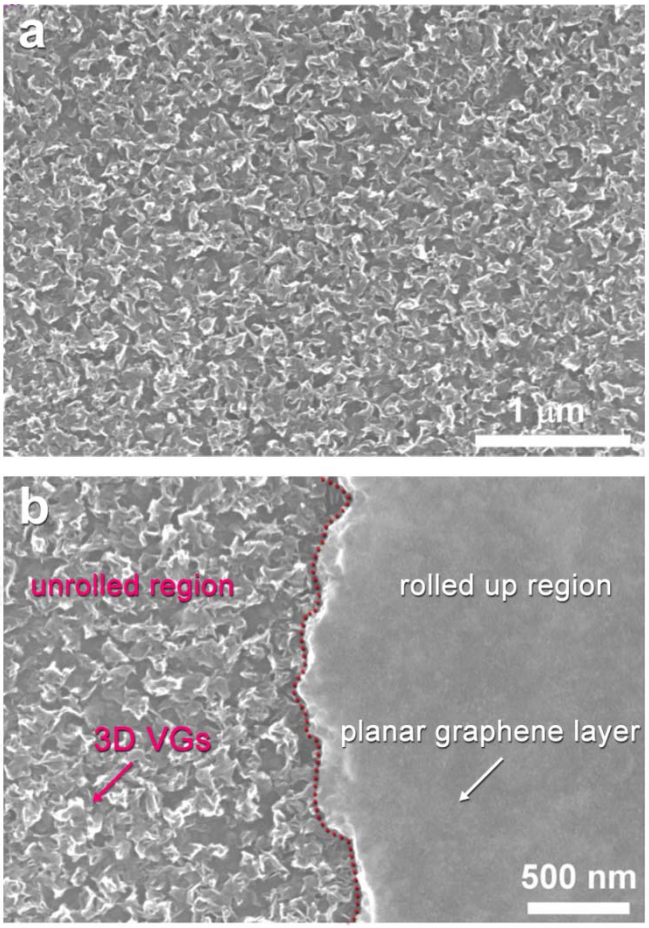

Figure S4. SEM comparison of the VGs and the intermediate layer of 2D graphene film. (a) SEM image of the unrolled VGs sample. (b) SEM image of the partially rolled VGs sample. **b** clearly demonstrates different morphologies of the obtained graphene sample, which gives an obvious comparison of the free-standing VGs (region on the left side of the dashed line) and the intermediate layer of 2D graphene film (region on the right side of the dashed line) between the upper VGs and the substrate.

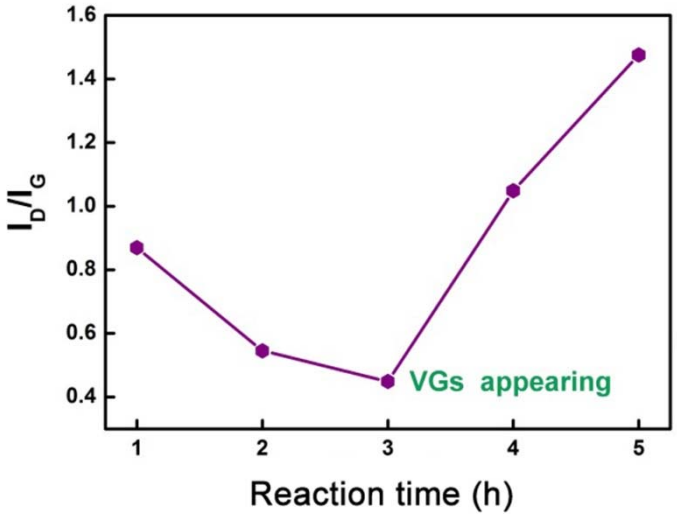

Figure S5. I_D/I_G value variation along with elongation of the reaction time.

In order to identify the density of defects, time-dependent Raman spectra of the VGs are performed. The ratio of I_D to I_G decreases in the realm of 1 to 3 h. After that, the ratio of I_D to I_G increases with extending the reaction time. This phenomenon indicates that the density of defects decreases along with graphene domain enlargement and then rapidly ascends after VGs evolution.

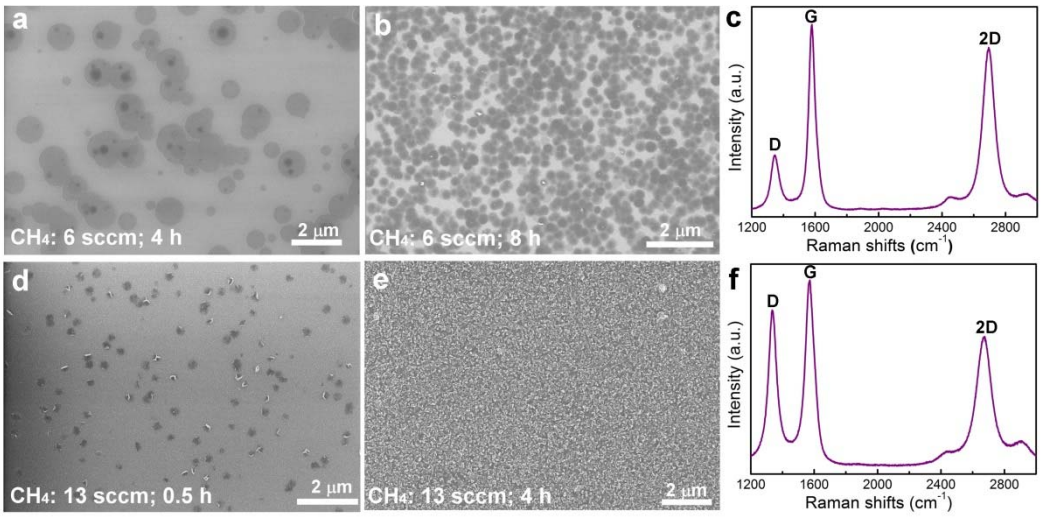

Figure S6. Influence of growth mode on ultimate graphene architecture. (a) Initial stage of graphene grown under low CH_4 flow rate (CH_4/H_2/Ar: 6/50/50 sccm, 4 h). (b) Extending reaction time of **a** to 8 h only generates few-layer plane graphene film composed by micrometer- or nanometer-graphene flakes randomly distributing on substrate surface. (c) Raman spectrum of graphene film in **b**. (d) Initial stage of graphene grown under ultrahigh CH_4 flow rate (CH_4/H_2/Ar: 13/50/50 sccm, 0.5 h). (e) Extending reaction time of **d** to 4 h yields large quantity of VGs on substrate. (f) Raman spectrum of VGs in **e**.

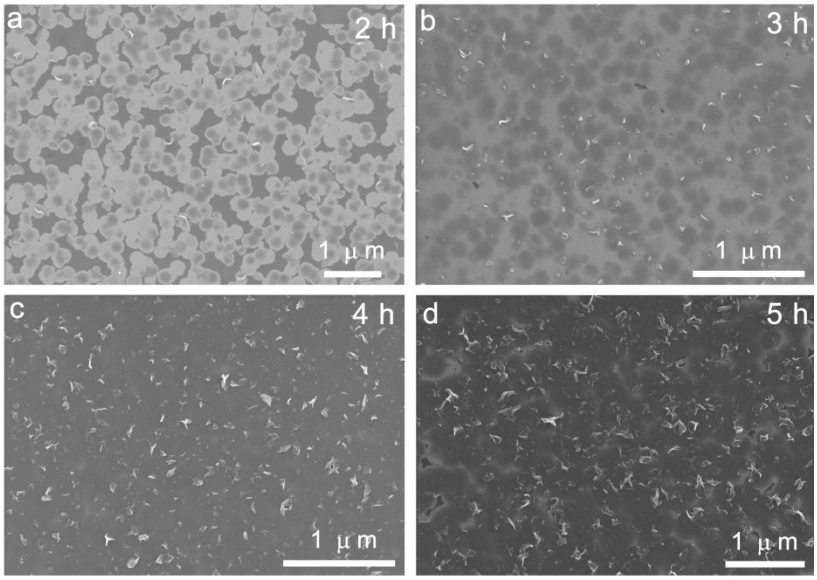

Figure S7. SEM images of graphene grown for different durationa at 7 sccm CH_4 where the transition of graphene growth from planar to vertical growth takes place. (a-d) SEM images of graphene grown for 2 h, 3 h, 4 h, and 5 h, respectively. The planar growth and vertical growth coexisted at 7 sccm CH_4, and the proportion of vertical graphene increased along the growth duration.

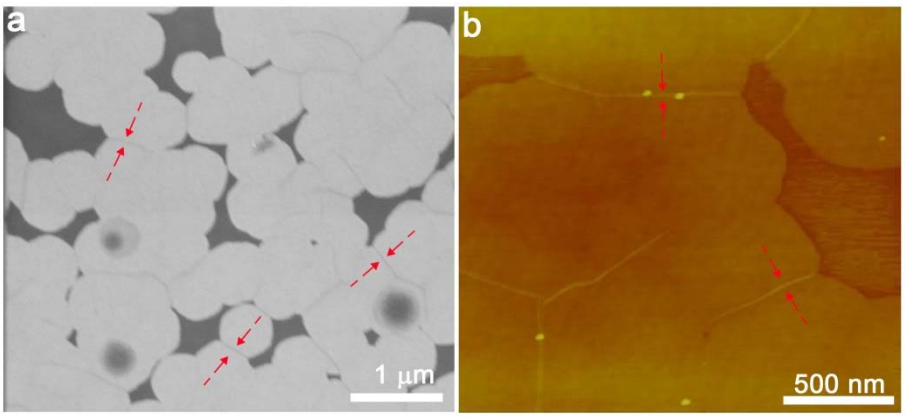

Figure S8. (a) SEM and (b) AFM image of graphene grain boundary formation by approaching graphene islands under low carbon source concentration. The adjacent individual graphene islands are marked by red arrows.

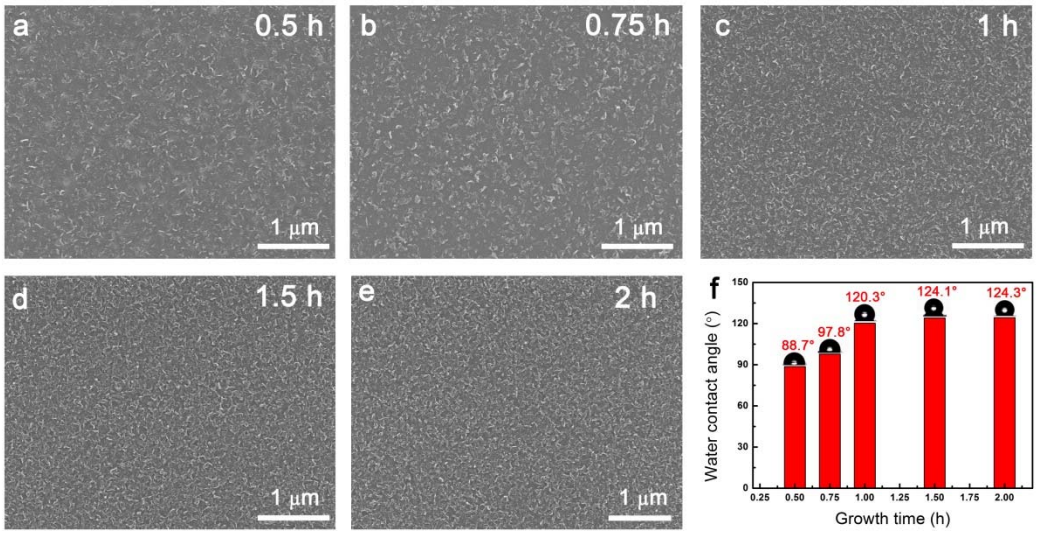

Figure S9. (a-e) SEM images of VGs grown for 0.5, 0.75, 1.0, 1.5 and 2.0 h, respectively. (f) Growth time of VGs and the static water contact angle corresponding to a-e. Conditions: 1130 °C under CH_4/H_2/Ar flow rates of 14/50/50 sccm.

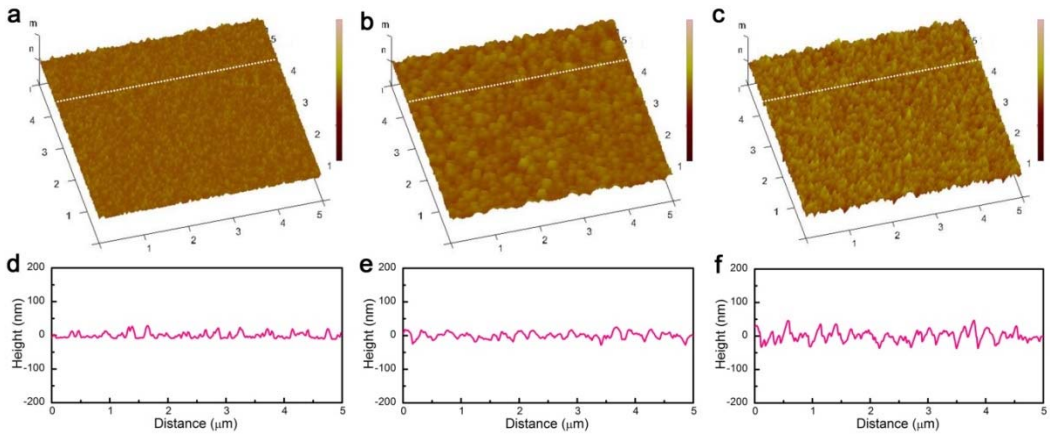

Figure S10. Height-engineering of VGs. (a-c) AFM 3D surface plots of VGs growth for 2, 4 and 6 h, respectively. (d-f) Corresponding height profiles of VGs in **a-c**. Conditions: VGs were grown at 10 sccm CH_4, 50 sccm H_2 and 50 sccm Ar for different times.

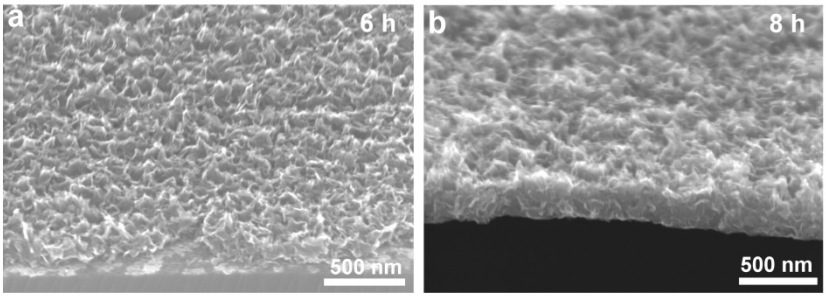

Figure S11. Influence of growth time on VGs height. (a) SEM image of VGs grown for 6 h under $CH_4/H_2/Ar$ of 10/50/50 sccm. (b) SEM image of VGs grown for 8 h under $CH_4/H_2/Ar$ of 10/50/50 sccm.

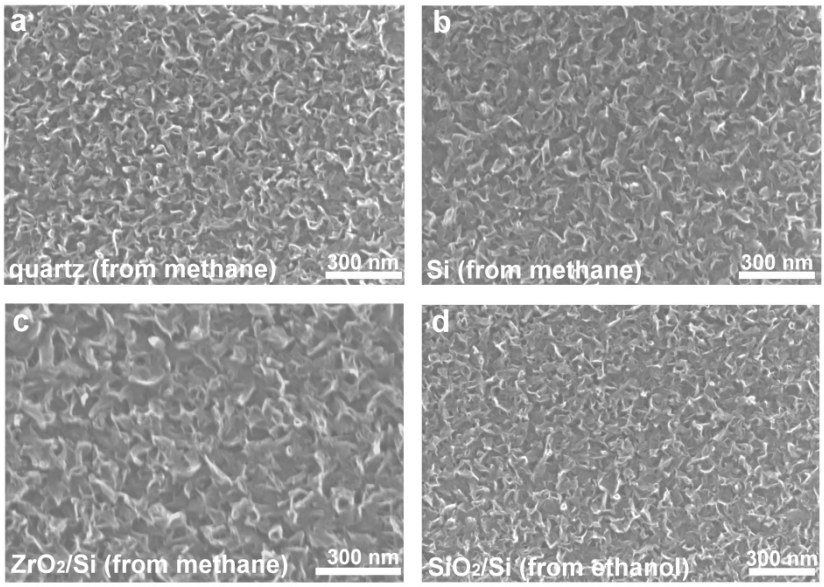

Figure S12. SEM images of VGs grown on various substrates and precursors. (a) VGs obtained by using CH_4 as carbon precursor on quartz. (b) VGs obtained by using CH_4 as carbon precursor on silicon. (c) VGs obtained by using CH_4 as carbon precursor on ZrO_2/Si. (d) VGs obtained by using ethanol as carbon precursor on SiO_2/Si. Conditions: VGs were grown at 8 sccm CH_4, 50 sccm H_2, and 50 sccm Ar for 6 h.

3. Supporting Tables

Table S1. Graphene growth mode investigation by varying the flow rate of CH_4.

Sample (#)	Growth temperature (°C)	CH_4 gas flow (sccm)	Ar gas flow (sccm)	H_2 gas flow (sccm)	Growth time (h)	Growth Mode
1	1130	3.0	50	50	10	PG
2	1130	5.0	50	50	5.0	PG
3	1130	5.5	50	50	5.0	PG
4	1130	6.0	50	50	5.0	PG
5	1130	6.5	50	50	3.0	PG
6	1130	6.5	50	50	5.0	PG
7	1130	7.0	50	50	3.0	PG + VG
8	1130	7.5	50	50	2.0	VG
9	1130	8.5	50	50	2.0	VG
10	1130	9.0	50	50	2.0	VG
11	1130	12	50	50	2.0	VG
12	1130	14	50	50	2.0	VG
13	1130	15	50	50	1.5	AC

PG: Planar Growth

VG: Vertical Growth

AC: Amorphous Carbon

PG + VG: Planar Growth with a small amount of Vertical Growth Graphene

Table S2. Graphene growth mode investigation by employing ethanol as carbon source.

Sample (#)	Growth temperature (°C)	H_2 gas flow (sccm)	Ar gas flow (sccm)	Growth time (h)	Growth Mode
1	1130	2	400	2.5	PG
2	1130	5	400	2.5	PG + VG
3	1130	10	400	2.5	PG + VG
4	1130	15	400	2.5	VG
5	1130	25	400	2.5	VG

PG: Planar Growth

VG: Vertical Growth

AC: Amorphous Carbon

PG + VG: Planar Growth with a small amount of Vertical Growth Graphene

Table S3. Comparison of the field emission performances of various graphene emitters.

Ref.	Method/Catalyst	Material	Turn-on electric field	Threshold electric field	Field-enhancement factor
[S3]	Electrophoretic deposition	r-GO	2.3 V/μm	5.2 V/μm	3700
[S4]	PECVD/Cu	VGs	1.3 V/μm	3.0 V/μm	1.1×10^4
[S5]	Template-guided CVD/Ni	Graphene-Si nanorod arrays	8 V/μm	n. a.	n. a.
[S6]	Photolithography	Graphene arrays	7.2 V/μm	n. a.	n. a.
[S7]	PECVD	N-doped VGs	1.05 V/μm	n. a.	3120/low-field; 17350/high-field
[S8]	CVD/Cu; spin-coating	CNTs on graphene	2.05 V/μm	2.2 V/μm	1023
[S9]	PECVD	VGs	2.23 V/μm	n. a.	5130
[S10]	PECVD/Ni	Graphene on ZnO NWs	1.3 V/μm	5.7 V/μm	1.5×10^4
[S11]	PECVD	VGs	4.7 V/μm	n. a.	n. a.
[S12]	PECVD	VGs	9.8 V/μm	n. a.	n. a.
[S13]	Hummers method	Screen-printed r-GO	1.5 V/μm	n. a.	4539
[S14]	Dry film scrolling	GO fibers	0.48 V/μm	0.62 V/μm	n. a.
[S15]	Template-guided CVD/Ni	Tubular graphene	n. a.	0.21-0.27 V/μm	$(1.7\text{-}1.9) \times 10^4$
[S16]	Hummers method	GO on Ni nanotip arrays	0.5 V/μm[a]	1 V/μm	n. a.
[S17]	Hummers method	GO on Si NWs	4 V/μm	n. a.	2024

[S18]	arc-discharge	N-doped graphene	0.6 V/μm	n. a.	49690 (the maximum)
[S19]	Radio frequency sputtering	VGs on CNTs	0.956 V/μm	1.497 V/μm	4398
[S20]	CVD/Cu	Graphene on ZnO NWs	5.4 V/μm[a]	n. a.	1100
[S21]	Thermal welding	Al-doped RGO	1.51 V/μm	2.18 V/μm	3048
[S22]	CVD/Cu	CNT-graphene film	2.9 V/μm	3.3 V/μm[b]	1373
[S23]	PECVD	VGs on CNT	0.87	1.54	5218
[S24]	PECVD/Cu	Graphene on Si NWs	2.01	3.22	6513
[S25]	Hydrothermal carbonization	Graphene on Ni/Si	2.0	3.2	3800
[S26]	PECVD/Ni	VGs on Graphene/ Ni foam	2.03 V/μm	n. a.	1294
[S27]	PECVD	N-doped VGs	4.6 V/μm	n. a.	1450
This work	**CVD**	**VGs**	**1.07 V/μm**	**1.65 V/μm**	**2550**

[a]Calculated at J = 10 mA/cm^2, while the E_{thres} of other literatures in this Table is calculated at J = 1 mA/cm^2;

[b]Calculated at J = 0.1 μA/cm^2, while the E_{on} of other literatures in this Table is calculated at J = 10 μA/cm^2;

[c]Calculated at J = 1 μA/cm^2, while the E_{on} of other literatures in this Table is calculated at J = 10 μA/cm^2;

[d]Calculated at J = 10 μA/cm^2, while the E_{thres} of other literatures in this Table is calculated at J = 1 mA/cm^2;

[e]Calculated at J = 0.1 mA/cm^2, while the E_{thres} of other literatures in this Table is calculated at J = 1 mA/cm^2;

GO: graphene oxide; NWs: nanowires; n. a.: not available.

4. Reference

(S1) Spanu, L.; Sorella, S.; Galli, G. Nature and Strength of Interlayer Binding in Graphite. *Phys. Rev. Lett.* **2009**, *103*, 196401.

(S2) Wei, G.; Penghao, X.; Graeme, H.; Kenneth, M. L.; Rui, H. Interfacial Adhesion between Graphene and Silicon Dioxide by Density Functional Theory with Van der Waals corrections. *J. Phys. D: Appl. Phys.* **2014**, *47*, 255301.

(S3) Wu, Z.-S.; Pei, S.; Ren, W.; Tang, D.; Gao, L.; Liu, B.; Li, F.; Liu, C.; Cheng, H.-M. Field Emission of Single-Layer Graphene Films Prepared by Electrophoretic Deposition. *Adv. Mater.* **2009**, *21*, 1756-1760.

(S4) Jiang, L.; Yang, T.; Liu, F.; Dong, J.; Yao, Z.; Shen, C.; Deng, S.; Xu, N.; Liu, Y.; Gao, H.-J. Controlled Synthesis of Large-Scale, Uniform, Vertically Standing Graphene for High-Performance Field Emitters. *Adv. Mater.* **2013**, *25*, 250-255.

(S5) Yen, W.-C.; Medina, H.; Hsu, C.-W.; Chueh, Y.-L. Conformal Graphene Coating on High-Aspect Ratio Si Nanorod Arrays by A Vapor Assisted Method for Field Emitter. *RSC Adv.* **2014**, *4*, 27106-27111.

(S6) Huang, C.-K.; Ou, Y.; Bie, Y.; Zhao, Q.; Yu, D. Well-Aligned Graphene Arrays for Field Emission Displays. *Appl. Phys. Lett.* **2011**, *98*, 263104.

(S7) Soin, N.; Sinha Roy, S.; Roy, S.; Hazra, K. S.; Misra, D. S.; Lim, T. H.; Hetherington, C. J.; McLaughlin, J. A. Enhanced and Stable Field Emission from in Situ Nitrogen-Doped Few-Layered Graphene Nanoflakes. *J. Phys. Chem. C* **2011**, *115*, 5366-5372.

(S8) Lahiri, I.; Verma, V. P.; Choi, W. An All-Graphene Based Transparent and Flexible Field Emission Device. *Carbon* **2011**, *49*, 1614-1619.

(S9) Qi, J. L.; Wang, X.; Zheng, W. T.; Tian, H. W.; Hu, C. Q.; Peng, Y. S. Ar Plasma Treatment on Few Layer Graphene Sheets for Enhancing Their Field Emission Properties. *J. Phys. D: Appl. Phys.* **2010**, *43*, 055302.

(S10) Zheng, W. T.; Ho, Y. M.; Tian, H. W.; Wen, M.; Qi, J. L.; Li, Y. A. Field Emission from a Composite of Graphene Sheets and ZnO Nanowires. *J. Phys. Chem. C* **2009**, *113*, 9164-9168.

(S11) Wang, J. J.; Zhu, M. Y.; Outlaw, R. A.; Zhao, X.; Manos, D. M.; Holloway, B. C.; Mammana, V. P. Free-Standing Subnanometer Graphite Sheets. *Appl. Phys. Lett.* **2004**, *85*, 1265-1267.

(S12) Pao, C. W.; Ray, S. C.; Tsai, H. M.; Chen, Y. S.; Chen, H. C.; Lin, I. N.; Pong, W. F.; Chiou, J. W.; Tsai, M. H.; Shang, N. G.; Papakonstantinou, P.; Guo, J. H. Change of Structural Behaviors of Organo-Silane Exposed Graphene Nanoflakes. *J. Phys. Chem. C* **2010**, *114*, 8161-8166.

(S13) Min, Q.; Tao, F.; Hui, D.; Lifeng, L.; Haibo, L.; Yiwei, C.; Zhuo, S. Electron Field Emission from Screen-Printed Graphene Films. *Nanotechnology* **2009**, *20*, 425702.

(S14) Cruz-Silva, R.; Morelos-Gomez, A.; Kim, H.-i.; Jang, H.-k.; Tristan, F.; Vega-Diaz, S.; Rajukumar, L. P.; Elías, A. L.; Perea-Lopez, N.; Suhr, J.; Endo, M.; Terrones, M. Super-Stretchable Graphene Oxide Macroscopic Fibers with Outstanding Knotability Fabricated by Dry Film Scrolling. *ACS Nano* **2014**, *8*,

5959-5967.

(S15) Nguyen, D. D.; Suzuki, S.; Kato, S.; To, B. D.; Hsu, C. C.; Murata, H.; Rokuta, E.; Tai, N.-H.; Yoshimura, M. Macroscopic, Freestanding, and Tubular Graphene Architectures Fabricated via Thermal Annealing. *ACS Nano* **2015**, *9*, 3206-3214.

(S16) Ye, D.; Moussa, S.; Ferguson, J. D.; Baski, A. A.; El-Shall, M. S. Highly Efficient Electron Field Emission from Graphene Oxide Sheets Supported by Nickel Nanotip Arrays. *Nano Lett.* **2012**, *12*, 1265-1268.

(S17) Devarapalli, R. R.; Kashid, R. V.; Deshmukh, A. B.; Sharma, P.; Das, M. R.; More, M. A.; Shelke, M. V. High Efficiency Electron Field Emission from Protruded Graphene Oxide Nanosheets Supported on Sharp Silicon Nanowires. *J. Mater. Chem. C* **2013**, *1*, 5040-5046.

(S18) Palnitkar, U. A.; Kashid, R. V.; More, M. A.; Joag, D. S.; Panchakarla, L. S.; Rao, C. N. R. Remarkably Low Turn-on Field Emission in Undoped, Nitrogen-Doped, and Boron-Doped Graphene. *Appl. Phys. Lett.* **2010**, *97*, 063102.

(S19) Deng, J.-h.; Zheng, R.-t.; Zhao, Y.; Cheng, G.-a. Vapor–Solid Growth of Few-Layer Graphene Using Radio Frequency Sputtering Deposition and Its Application on Field Emission. *ACS Nano* **2012**, *6*, 3727-3733.

(S20) Yang, Z.; Zhao, Q.; Ou, Y.; Wang, W.; Li, H.; Yu, D. Enhanced Field Emission from Large Scale Uniform Monolayer Graphene Supported by Well-Aligned ZnO Nanowire Arrays. *Appl. Phys. Lett.* **2012**, *101*, 173107.

(S21) Jeong, H. J.; Jeong, H. D.; Kim, H. Y.; Kim, S. H.; Kim, J. S.; Jeong, S. Y.; Han, J. T.; Lee, G.-W. Flexible Field Emission from Thermally Welded Chemically Doped Graphene Thin Films. *Small* **2012**, *8*, 272-280.

(S22) Nguyen, D. D.; Tai, N.-H.; Chen, S.-Y.; Chueh, Y.-L. Controlled Growth of Carbon Nanotube-Graphene Hybrid Materials for Flexible and Transparent Conductors and Electron Field Emitters. *Nanoscale* **2012**, *4*, 632-638.

(S23) Deng, J.-H.; Deng, L.-N.; Liu, R.-N.; Han, A. L.; Li, D.-J.; Cheng, G.-A. Vapor-Solid Preparation of Densely Distributed and Small-Sized Graphene Nanoflakes on One-Dimensional Nanomaterials for Low-Field and Highly Stable Field Emission. *Carbon* **2016**, *102*, 1-9.

(S24) Lv, S.; Li, Z.; Liao, J.; Wang, G.; Li, M.; Miao, W. Optimizing Field Emission Properties of the Hybrid Structures of Graphene Stretched on Patterned and Size-controllable SiNWs. *Sci. Rep.* **2015**, *5*, 15035.

(S25) Khare, R. T.; Gelamo, R. V.; More, M. A.; Late, D. J.; Rout, C. S. Enhanced Field Emission of Plasma Treated Multilayer Graphene. *Appl. Phys. Lett.* **2015**, *107*, 123503.

(S26) Cheng, L.; Qu, L.; Deng, J.-H. High-Efficiency Field Emission from Pressed Nickel Foam-Flat Graphene-Vertical Graphene Hybrids. *Mater. Lett.* **2016**, *176*, 165-168.

(S27) Zhao, C. X.; Zhang, Y.; Deng, S. Z.; Xu, N. S.; Chen, J. Surface Nitrogen Functionality for the Enhanced Field Emission of Free-Standing Few-Layer Graphene Nanowalls. *J. Alloys Compd.* **2016**, *672*, 433-439.